CHIN. PHYS. LETT. Vol. 30, No. 7 (2013) 074302

Modeling of Shock Wave Generated from a Strong Focused Ultrasound Transducer *

CHEN Tao(陈涛)[1,3], QIU Yuan-Yuan(邱媛媛)[2], FAN Ting-Bo(范庭波)[3], ZHANG Dong(章东)[1**]

[1]*Key Laboratory of Modern Acoustics, Nanjing University, Nanjing 210093*
[2]*School of Electronic Information, Nantong University, Nantong 226019*
[3]*Jiangsu Province Institute for Medical Equipment Testing, Nanjing 210012*

(Received 16 February 2013)

A combined time and frequency domain method is developed for the calculation of a shock wave induced by a strong focused ultrasound transducer in the oblate spheroidal coordinate system. The spheroidal beam equation (SBE) is utilized to describe the nonlinear sound propagation; the diffraction and attenuation effects are calculated in the frequency-domain, while the nonlinear effect is calculated in the time-domain. Compared with the traditional frequency-domain method, this method could calculate the shock wave effectively without oscillation at the shock front and with less computation time. When the harmonic number is 200, the computation time by this method is about 1/16 of that used by the traditional frequency-domain method.

PACS: 43.25.+y, 43.80.+p DOI: 10.1088/0256-307X/30/7/074302

High intensity focused ultrasound (HIFU) is a noninvasive treatment that focuses high intensity ultrasound energy to the target area of tissue within the body with little damage to the intervening tissue.[1,2] This technique has been used clinically for ablating solid tumors of the prostate, liver, breast, kidney, and brain, etc.[2–5] Modeling of the nonlinear acoustic distribution is important for accurately predicting and quantifying tissue response to focused ultrasound. The well-known Khokhlov–Zabolotskaya–Kuznetsov (KZK) equation is widely used, which takes account of the combined effects of diffraction, attenuation and nonlinearity.[6] Its numerical computation could be implemented either in time or in frequency domain.[7–10] However, the KZK equation cannot accurately describe the acoustic field generated from the strong focused transducer with the wide half-aperture larger than 16° due to the paraxial approximation.[11] Much attention has been paid to the research of transducers with a wide aperture angle, owing to their advantage of ensuring high ultrasonic intensity for a short time to reach a required thermal dose. Kamakura *et al.* developed a spheroidal beam equation (SBE) for the theoretical prediction for strong focused ultrasonic beams from a circular transducer with a large aperture angle.[12] Generally, this equation could be calculated in the frequency domain with an operator splitting procedure.[7,13,14] However, as the applied acoustic power increases, several hundreds of harmonics are required in the computation owing to the generation of the shock wave. As a result, there could be oscillations near the shock front, and huge computation cost. Recently, a Godunov-type shock capturing method has been utilized to calculate the strong nonlinear effect in the KZK equation.[15] In this Letter, the acoustic field of a strong focused ultrasound is calculated with a combined time- and frequency-domain method. The SBE governs the ultrasound propagation. The numerical computation is performed with the calculations of diffraction and attenuation effects in the frequency-domain and the nonlinear effect in the time-domain with a Godunov-type scheme finite-difference method.[16,17]

The SBE is employed to describe the nonlinear ultrasound propagation in the oblate spheroidal coordinate with $-\infty < \sigma < +\infty$, $0 < \eta < 1$ and $0 \leq \phi \leq 2\pi$. The variables (σ, η, ϕ) are related to the rectangular coordinate (x, y, z) with $x = b[(1+\sigma^2)(1-\eta^2)]^{1/2}\cos\phi$, $y = b[(1+\sigma^2)(1-\eta^2)]^{1/2}\sin\phi$, and $z = b\sigma\eta$, in which $2b$ is the interfocal length. The focused ultrasound field is divided into two regions, i.e., $\sigma < \sigma_0$ and $\sigma \geq \sigma_0$, where σ_0 denotes a specific transition location. The former is close to the source where spherically converging waves predominate and the spherical coordinates are preferable; the latter is near the focus where the paraxial or planar parabolic approximation is useful. Two separate equations are used to describe the spheroidal wave and planar wave

*Supported by the National Basic Research Program of China under Grant No 2011CB707900, the National Natural Science Foundation of China under Grant Nos 81127901, 11174141, 81227004, 11204144 and 11161120324, the Natural Science Foundation of Jiangsu Province under Grant Nos BE2011110 and BK2012226, the National High-Technology Research and Development Program of China under Grant No 2012AA022700, and the State Key Laboratory of Acoustics of Chinese Academy Sciences.

**Corresponding author. Email: dzhang@nju.edu.cn

© 2013 Chinese Physical Society and IOP Publishing Ltd

in the two regions,[12,18]

$$\begin{aligned}
&\frac{\partial^2 P}{\partial\tau_{\rm s}\partial\sigma}+\frac{1}{2}\frac{\sin 2\theta}{\sigma(1+\sigma^2)}\frac{\partial^2 P}{\partial\tau_{\rm s}\partial\theta}\\
&+\frac{\varepsilon\sqrt{\sigma^2+\sin^2\theta}}{\sigma(1+\sigma^2)}\Big(\frac{\partial^2 P}{\partial\theta^2}+\cot\theta\frac{\partial P}{\partial\theta}\Big)+\frac{E}{\sigma}\frac{\partial P}{\partial\tau_{\rm s}}\\
&=-\frac{\sqrt{\sigma^2+\sin^2\theta}}{\sigma}\Big(\alpha b\frac{\partial^3 P}{\partial\tau_{\rm s}^3}+\frac{b}{2l_{\rm D}}\frac{\partial^2 P^2}{\partial\tau_{\rm s}^2}\Big)E,\\
&\qquad\qquad(\sigma<\sigma_0<0);\\
&\frac{\partial^2 P}{\partial\tau_{\rm p}\partial\sigma}-\frac{\sigma\sin\theta}{1+\sigma^2}\frac{\partial^2 P}{\partial\tau_{\rm p}\partial\theta}\\
&-\frac{\varepsilon\Big(2-\cos\theta\Big)}{1+\sigma^2}\Big(\frac{\partial^2 P}{\partial\theta^2}+\cot\theta\frac{\partial P}{\partial\theta}\Big)\\
&=\Big(\alpha b\frac{\partial^3 P}{\partial\tau_{\rm p}^3}+\frac{b}{2l_{\rm D}}\frac{\partial^2 P^2}{\partial\tau_{\rm p}^2}\Big)E,\quad(\sigma\geq\sigma_0).
\end{aligned}\tag{1}$$

Owing to the axial symmetry of the transducer, the variable ϕ is omitted in Eq. (1). The angle variable θ is related to η as $\eta=\cos\theta$. The character ε is set to be $1/2kb$ and E is a function of σ and θ as $E(\sigma,\theta)=(\sigma^2+\cos 2\theta)/(1+\sigma^2)$. $\tau_{\rm s}=\omega[t+b(\sigma^2+\sin 2\theta)^{1/2}/c_0]$ is the spherically retarded time near the source, and $\tau_{\rm p}=\omega[t-b\sigma\cos\theta/c_0]$ is the retarded time for the planar wave near the focus. $P=p/p_0$ is the normalized sound pressure, where p_0 is the amplitude of sound pressure on the source surface, c_0 is the sound speed, ρ_0 is the density of medium, β is the nonlinear coefficient of medium, k is the wave number, $l_{\rm D}=\rho_0 c_0^3/\beta p_0\omega$ is the shock formation distance for a planar wave, $\alpha=\delta\omega^2/2c_0^3$ is the sound attenuation coefficient, with δ being the sound diffusivity and ω the angular frequency.

This equation is numerically solved by a combined time- and frequency-domain method to deal with the generation of the shock wave. With the operator splitting procedure, Eq. (1) could be separated into the following two equations,

$$\begin{aligned}
\frac{\partial^2\bar{p}}{\partial\tau\partial\sigma}=&G\Big(\sigma,\theta\Big)\frac{\partial^2 P}{\partial\tau\partial\theta}+H(\sigma,\theta)\Big(\frac{\partial^2 P}{\partial\theta^2}+\cot\theta\frac{\partial P}{\partial\theta}\Big)\\
&+R(\sigma,\theta)\frac{\partial P}{\partial\tau}+S(\sigma,\theta)\frac{\partial^3 P}{\partial\tau^3},
\end{aligned}\tag{2}$$

$$\frac{\partial P}{\partial\sigma}=N(\sigma,\theta)\frac{\partial P^2}{\partial\tau},\tag{3}$$

where $G(\sigma,\theta)$, $H(\sigma,\theta)$, $R(\sigma,\theta)$, $S(\sigma,\theta)$ and $N(\sigma,\theta)$ are coefficients that can be derived from Eq. (1), and their values are different for $\sigma<\sigma_0$ and $\sigma\geq\sigma_0$. Equation (2) is calculated in the frequency domain with the boundary condition at the axial distance σ. Then utilizing the results from Eq. (2) as the new boundary conditions at the axial distance σ, Eq. (3) is calculated in the time domain, and the derived results are the solutions at the distance $\sigma+d\sigma$. The sound pressures near the source and the focus are represented as the following Fourier series expansions, respectively.

$$\begin{aligned}
P&=\sum_{n=-\infty}^{\infty}C_n^{(\rm s)}\exp(jn\tau_{\rm s}),\ \sigma<\sigma_0<0,\\
P&=\sum_{n=-\infty}^{\infty}C_n^{(\rm p)}\exp(jn\tau_{\rm p}),\ \sigma\geq\sigma_0,
\end{aligned}\tag{4}$$

where $C_n^{(\rm s)}$ and $C_n^{(\rm p)}$ are the complex amplitudes of the nth harmonic. Substituting Eq. (4) into Eq. (2), a set of coupled differential equations is derived and calculated by a finite-difference implicit backward algorithm for each harmonic.

Equation (3) is solved in the time-domain with the NT scheme finite-difference method.[16] In this equation, the variable θ could be treated as a constant. The sliding average of $P(\sigma,\tau)$ in the τ direction is written as[16]

$$\bar{P}(\sigma,\tau)=\frac{1}{d\tau}\int_{\tau-d\tau/2}^{\tau+d\tau/2}P(\sigma,t)dt.\tag{5}$$

The linear approximation to the solution at the distance $\sigma=m\times d\sigma$, and in the time interval $(j\pm 1/2)d\tau$ is

$$\begin{aligned}
P(m\times d\sigma,\tau)\approx&\bar{P}_j^m+(P_\tau)_j^m(\tau-j\times d\tau),\\
&|\tau-j\times d\tau|\leq\frac{d\tau}{2},
\end{aligned}\tag{6}$$

where $\bar{P}_j^m$ represents $\bar{P}(m\times d\sigma, j\times d\tau)$. The time derivative of $P(\sigma,\tau)$ is obtained by

$$\begin{aligned}
(P_\tau)_j^m=&\min_\mathrm{mod}\Big(\frac{P_j^m-P_{j-1}^m}{d\tau},\frac{P_{j+1}^m-P_{j-1}^m}{2d\tau},\\
&\frac{P_{j+1}^m-P_j^m}{d\tau}\Big),
\end{aligned}\tag{7}$$

where the min_mod function is defined by

$$\min_\mathrm{mod}(x_1,x_2,\ldots)=\begin{cases}\min_j(x_j), & \text{if } x_j>0\forall j,\\ \max_j(x_j), & \text{if } x_j<0\forall j,\\ 0, & \text{otherwise,}\end{cases}\tag{8}$$

$\bar{P}_j^{m+1}$ is calculated by the NT scheme,

$$\begin{aligned}
\bar{P}_{j+1/2}^{m+1}=&\frac{\bar{P}_j^m+\bar{P}_{j+1}^m}{2}+\frac{d\tau}{8}((P_\tau)_j^m-(P_\tau)_{j+1}^m)\\
&-\frac{d\sigma}{d\tau}[f(P_{j+1}^{m+1/2})-f(P_j^{m+1/2})],
\end{aligned}\tag{9}$$

where $f(P)=-N(\sigma,\theta)P^2$ is the nonlinear term, and the midpoint values, $P_j^{m+1/2}$, are predicted by Taylor expansion,

$$P_j^{m+1/2}=\bar{P}_j^m-\frac{d\sigma}{2}\Big(\frac{\partial f}{\partial\tau}\Big)_j^m.\tag{10}$$

Thus, the solution at the next distance level $\sigma = (m+1) \times d\sigma$ is derived by its staggered cell averages, $\bar{P}_{j+1/2}^{m+1}$. [16]

Initial value of $C_n^{(\mathrm{s})}$ at $\sigma = \sigma_{\max}$ is given as the boundary condition,

$$C_n^{(\mathrm{s})} = \begin{cases} -0.5j, & (0 \le \theta < \theta_0), \\ 0, & (\theta_0 \le \theta < \pi/2), \end{cases} \tag{11}$$

where $\theta \le \theta_0$ is the transducer surface region, and $\theta_0 = \tan^{-1}(\frac{\tan\alpha_0}{\sqrt{1+1/\sigma_{\max}^2}})$. The relationship between $C_n^{(\mathrm{s})}$ and $C_n^{(\mathrm{p})}$ at $\sigma = \sigma_0$ is as follows:

$$C_n^{(\mathrm{p})} = C_n^{(\mathrm{s})} \exp(jnkb(\sqrt{\sigma_0^2 + \sin^2\theta} + \sigma_0 \cos\theta)). \tag{12}$$

In the numerical simulation, a strong focusing spherical transducer is employed, the geometric parameters of which are: radius $a = 5.0\,\mathrm{cm}$, focal length $F = 10.3\,\mathrm{cm}$, the central frequency $f_0 = 1.1\,\mathrm{MHz}$. The geometric relationship between the transducer and the oblate spheroidal coordinate is illustrated in Fig. 1. Physical parameters of water used for calculation are: $\rho_0 = 1000\,\mathrm{kg/m^3}$, $c_0 = 1500\,\mathrm{m/s}$, $\alpha = 0.025\,\mathrm{Np/m/MHz^2}$, $\beta = 3.5$. In the numerical simulation, $\sigma_{\max}$ and σ_0 are set as 4.0 and -0.5, respectively. The computation region ranges from 0 to $\pi/2$ on the θ-axis and from $-\sigma_{\max}$ to the observer on the σ-axis. 1000 grid points are set from 0 to $\pi/2$ on the θ-axis, thus the step size of θ is 1.57×10^{-3} radian. The step size in σ direction is 1.0×10^{-3}. For a strongly nonlinear situation, the series number must be increased and step size should be decreased at the same time. The maximum series number used for Fourier series expansion when the shock wave appears in Eq. (4) is set to be 2048 in this study.

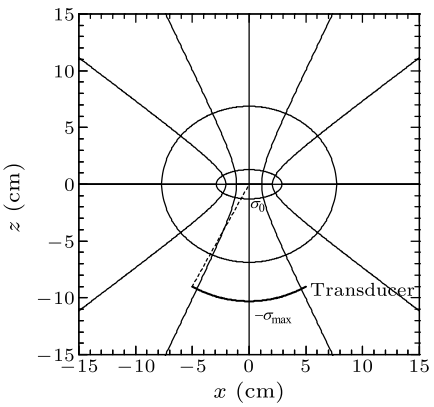

Fig. 1. Illustration of the transducer and the oblate spheroidal coordinate.

The parameters $\sigma_{\max}$ and σ_0 in the SBE model are set artificially. To examine the validity of the parameters, the simulation results are compared with the Rayleigh integral results in the linear case (the nonlinear coefficient is set as 0). Figures 2(a) and 2(b) show the normalized pressures along the axial and the radial directions, respectively, where the solid line and the dashed line represent numerical results from Rayleigh integral and SBE model, respectively. It is observed that the results from SBE model coincide well with that from Rayleigh integral in the focal region.

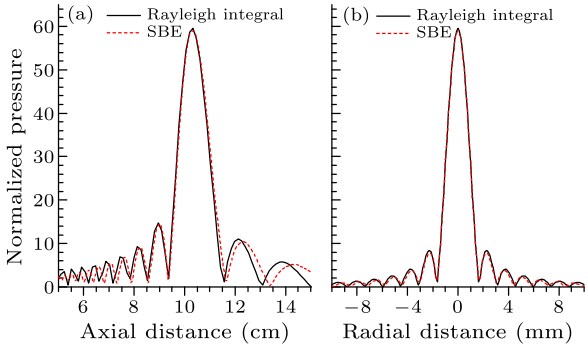

Fig. 2. The linear axial (a) and radial (b) normalized sound pressures obtained by Rayleigh integral (solid line) and SBE solution (dashed line).

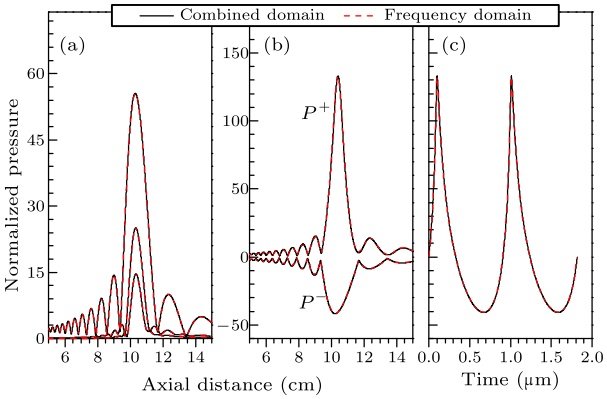

Fig. 3. Comparison of the numerical calculations in the combined domain and the frequency domain: (a) the axial pressure profiles of the fundamental, second and third harmonics, (b) the axial peak positive and negative pressure profiles, (c) the focal waveform. The solid and dashed lines represent the combined domain method and the traditional frequency-domain method respectively.

The simulated results in the combined domain are then compared with those obtained by the traditional frequency-domain method. The pressure amplitude on the source surface is set to be 200 kPa. Figure 3 plots the axial pressures of the fundamental, second and third harmonics (Fig. 3(a)), the peak positive and negative pressure profiles (Fig. 3(b)), and the focal waveform (Fig. 3(c)), where the solid and dashed lines represent the results obtained by the combined domain method and the traditional frequency-domain method. The agreement of the calculated results indicates that the calculation in the combined domain can accurately predict the nonlinear generation.

Finally, the simulations of the shock wave gen-

eration are examined. Figure 4(a) shows the axial peak positive and negative pressure profiles, and the focal waveform when the pressure amplitude on the source surface is 350 kPa. The normalized peak positive and negative pressure amplitudes (normalized by the source pressure amplitude) are 209 and 35, respectively. Figure 4(b) shows the normalized focal waveform in time domain, indicating that the focal pressure changes from 2.6 to 209 in 1.9 ns.

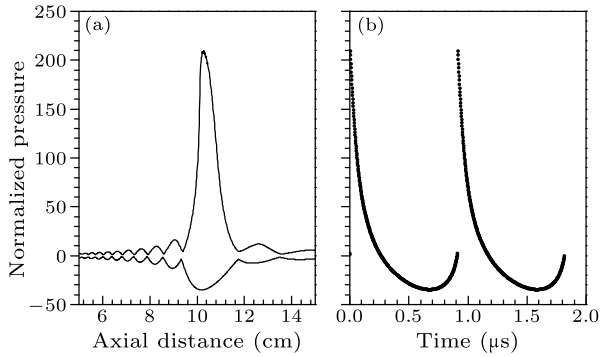

Fig. 4. Simulated results at source pressure amplitude 350 kPa by using the combined domain method: (a) the axial peak positive and negative pressure profiles, (b) the focal waveform in time domain.

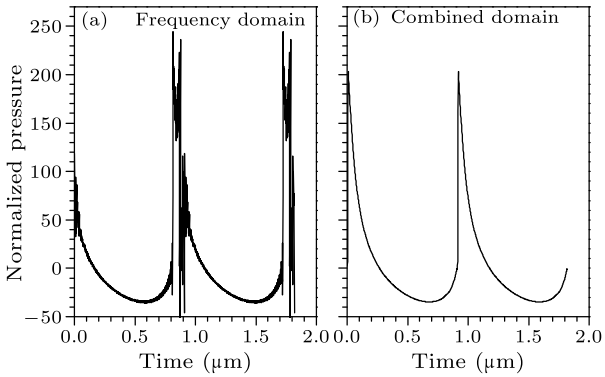

Fig. 5. The focal waveforms for the source amplitude 350 kPa and the number of harmonics is 200: (a) calculated by the frequency domain method, and (b) calculated by the combined domain method.

Compared with the traditional frequency-domain method, the combined time- and frequency-domain method has two advantages for calculating shock wave, i.e., smoother waveform and less computation time. Figure 5 compares the focal waveform calculated by using the two methods when the source pressure amplitude is 350 kPa. The series number used for Fourier series expansion is 200. Obviously, the waveform by the frequency-domain method (Fig. 5(a)) is not stable near the shock front. By contrast, the waveform by the combined time- and frequency-domain method (Fig. 5(b)) is stable and becomes a smooth waveform. In addition, the computation time by the combined time- and frequency-domain method is much shorter (1/16) than that by the traditional frequency-domain method when the maximum harmonic number is 200.

In conclusion, a combined time- and frequency-domain method is proposed for the calculation of shock wave in the oblate spheroidal coordinate system. By this approach, the diffraction and attenuation effects are calculated in the frequency-domain, while the nonlinear effect is calculated in the time-domain. The validity of this approach has been examined by the linear case and the relative low nonlinear case. Then this approach is extended to compute the shock wave. Compared with the traditional frequency-domain method, this method shows advantages of low computation cost and no oscillation at the shock front.

References

[1] Kennedy J E 2005 *Nat. Rev. Cancer* **5** 321
[2] Zhang Z, Chen T and Zhang D 2013 *Chin. Phys. Lett.* **30** 024302
[3] ter Haar G and Coussios C 2007 *Int. J. Hyperthermia* **23** 89
[4] Illing R O, Kennedy J E, Wu F, ter Haar G R, Protheroe A S, Friend P J, Gleeson F V, Cranston D W, Phillips R R and Middleton M R 2005 *Br. J. Cancer* **93** 890
[5] Wu F, Wang Z B, Chen W Z, Zou J Z, Bai J, Zhu H, Li K Q, Jin C B, Xie F L and Su H B 2005 *Radiology* **235** 659
[6] Aanonsen S I, Barkve T et al 1984 *J. Acoust. Soc. Am.* **75** 749
[7] Khokhlova V A, Bailey M R, Reed J A, Cunitz B W, Kaczkowski P J and Crum L A 2001 *J. Acoust. Soc. Am.* **110** 95
[8] Yang X and Cleveland R O 2005 *J. Acoust. Soc. Am.* **117** 113
[9] Liu Z B, Fan T B and Zhang D 2010 *Chin. Phys. Lett.* **27** 094303
[10] Lee Y S and Hamilton M F 1995 *J. Acoust. Soc. Am.* **97** 906
[11] Tjøtta J N, Tjøtta S and Vefring E H 1991 *J. Acoust. Soc. Am.* **89** 1017
[12] Kamakura T, Ishiwata T and Matsuda K 2000 *J. Acoust. Soc. Am.* **107** 3035
[13] Fan T B, Liu Z B, Zhang Z and Zhang D 2009 *Chin. Phys. Lett.* **26** 084302
[14] Canney M S, Bailey M R, Crum L A, Khokhlova V A and Sapzhnikov O A 2008 *J. Acoust. Soc. Am.* **124** 2406
[15] Canney M S, Khokhlova V A, Bessonova O V, Bailey M R and Crum L A 2010 *Ultrasound Med. Biol.* **36** 250
[16] Kurganov A and Tadmor E 2000 *J. Comput. Phys.* **160** 241
[17] Nessyahu H and Tadmor E 1990 *J. Comput. Phys.* **87** 408
[18] Liu M H, Zhang D and Gong X F 2007 *Chin. Phys. Lett.* **24** 2267